Cell Reports
Resource

Cell PRESS
Open ACCESS

A Comprehensive Wiring Diagram of the Protocerebral Bridge for Visual Information Processing in the *Drosophila* Brain

Chih-Yung Lin,[1] Chao-Chun Chuang,[3,4] Tzu-En Hua,[1] Chun-Chao Chen,[1] Barry J. Dickson,[5] Ralph J. Greenspan,[6] and Ann-Shyn Chiang[1,2,6,7,*]
[1]Institute of Biotechnology and Department of Life Science
[2]Brain Research Center
National Tsing Hua University, Hsinchu 30013, Taiwan
[3]National Center for High-Performance Computing, Hsinchu 30076, Taiwan
[4]Institute of Bioinformatics and Systems Biology, National Chiao Tung University, Hsinchu 30010, Taiwan
[5]Institute of Molecular Pathology, Dr. Bohr-gasse 7, A-1030 Vienna, Austria
[6]Kavli Institute for Brain and Mind, University of California at San Diego, La Jolla, CA 92093-0126, USA
[7]Genomics Research Center, Academia Sinica, Nankang, Taipei 11529, Taiwan
*Correspondence: aschiang@life.nthu.edu.tw
http://dx.doi.org/10.1016/j.celrep.2013.04.022

SUMMARY

How the brain perceives sensory information and generates meaningful behavior depends critically on its underlying circuitry. The protocerebral bridge (PB) is a major part of the insect central complex (CX), a premotor center that may be analogous to the human basal ganglia. Here, by deconstructing hundreds of PB single neurons and reconstructing them into a common three-dimensional framework, we have constructed a comprehensive map of PB circuits with labeled polarity and predicted directions of information flow. Our analysis reveals a highly ordered information processing system that involves directed information flow among CX subunits through 194 distinct PB neuron types. Circuitry properties such as mirroring, convergence, divergence, tiling, reverberation, and parallel signal propagation were observed; their functional and evolutional significance is discussed. This layout of PB neuronal circuitry may provide guidelines for further investigations on transformation of sensory (e.g., visual) input into locomotor commands in fly brains.

INTRODUCTION

One of most challenging issues in the field of sensory neuroscience is understanding how sensory coding is represented from the outside world and conveyed into the brain to orchestrate complex behaviors (Bargmann, 2006). Neural circuits can be reconstructed from a single brain through resolving synaptic connections and segmenting individual neurons directly from serial electron microscopic images (Briggman and Denk, 2006). However, labor intensive identification of large numbers of neural structures makes this approach practical only for a tiny piece of brain tissue (Seung, 2009). Alternatively, by labeling a few single neurons with mosaic analysis with a repressible cell marker (MARCM) and then combining these neurons across multiple brains, we have recently established an open access database, FlyCircuit, that contains ~16,000 individual neurons in a standard *Drosophila* adult brain (Lee and Luo, 1999; Lin et al., 2007; Chiang et al., 2011). This brainwide wiring map has allowed researchers to formulate hypotheses about information flow in the *Drosophila* brain and also to guide genetic manipulations aimed at understanding how genes and circuits orchestrate complex behaviors.

The central complex (CX), composed of the protocerebral bridge (PB), the fan-shaped body (FB), the ellipsoid body (EB), and the noduli (No), is an integration center receiving inputs from many parts of the brain for controlling visual and locomotion related behaviors in all arthropods, including crayfish and insects (Homberg, 2008). In *Drosophila*, morphological analysis from Golgi impregnation and *Gal4* expression revealed more than 50 types of CX neurons belonging to small or large field neurons (Hanesch et al., 1989; Renn et al., 1999; Young and Armstrong, 2010a, 2010b). These are defined as superclasses in the current study (see below). *Drosophila* PB neurons have been shown to form 16 glomeruli connected to substructures within the CX and to the CX accessory regions called ventral bodies (VBOs) and lateral triangle (LT) (Hanesch et al., 1989; Young and Armstrong, 2010b). Accumulating evidence from structural lesions and electrophysiological studies has established a role for the PB in various functions such as the topographic representation of E-vector orientation in locusts (Heinze and Homberg, 2007), integration of skylight cues in butterflies (Heinze and Reppert, 2011), and visual targeting and control of step-length in walking *Drosophila* (Strauss, 2002; Triphan et al., 2010).

In the following article, by compiling individual single neurons labeled with polarity markers into a volume model of the CX, we have constructed a comprehensive map of PB circuits indicating the putative direction of information flow. Our analysis reveals

CrossMark

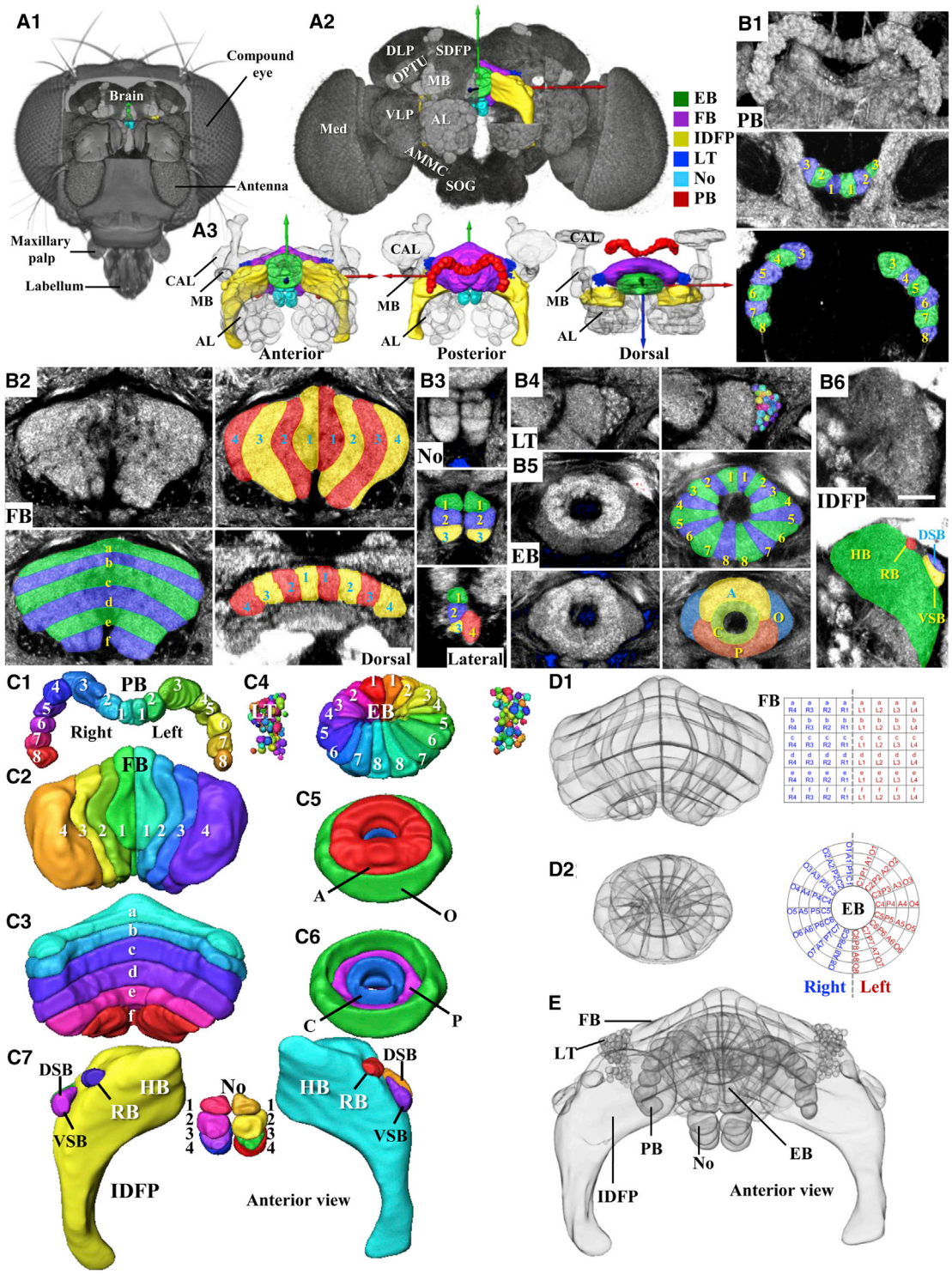

Figure 1. Building a Volume Model of the CX

(A) Gross anatomy of the CX. The CX located at the center of the fly head (A1), is embedded behind the paired MBs and ALs. Spatial location of the CX is revealed by digitally removing parts of the left MB and AL (A2). Spatial relationships among CX neuropils are visualized from anterior, posterior, and dorsal views with three axes parallel to the principal axes of the brain (A3).

(B) Segmentation of CX subunits. Imaging of anti-DLG stained neuropils (gray) revealed distinct structural boundaries, including subunits within the PB (B1), FB (B2), No (B3), LT (B4), EB (B5), and IDFP (B6). Each color represents a demarcated subunit within the structure. Pictures are mostly frontal views, unless otherwise specified, of confocal projections of several adjacent optical sections.

(legend continued on next page)

194 distinct types of PB neurons that follow highly ordered wiring principles.

RESULTS

Analytical Strategy

We describe below a cell-by-cell analysis of the wiring and predicted connectivity of the CX. The analysis is based on images of single neurons innervating the PB. Because the following description of results is intricate, we first present, as an aid to comprehension, an outline of the strategy used. First, we build a volume model of the CX and its substructures to provide a context in which to place each of the neurons. Next, we set up a system for classification of all PB neurons into categories based on their putative dendrite-axon polarities and innervation patterns. Then we sequentially describe the varieties of local neurons (LNs) within the PB, the inputs to the PB, and the outputs from the PB. Finally, we present our models of information flow in the CX based on inferred connectivity patterns.

Building a Volume Model of the CX

In order to archive PB neurons for comparative analysis, we have generated a CX volume model serving as a three-dimensional (3D) framework for fine tuning the spatial distribution of PB neurons by means of local structural alignment. High-resolution confocal imaging of sample brains immunostained with anti-discs large (DLG), which labels septate junctions, revealed distinct boundaries between CX areas and subunits within them (Figure 1B) (Woods and Bryant, 1991). By manually demarking the boundaries of CX substructure, we have generated a CX volume model (Figure 1C). Our nomenclature, with systematic abbreviations, follows previous reports whenever possible, except where there are conflicts (Figure 1D; Table S1). For example, R and L are used to indicate right and left hemispheres, numbers are used to indicate horizontal subunits and small letters are used to indicate vertical subunits. This CX volume model was then used to catalog individual PB neurons derived from different brain samples (Figure 1E; Movie S1). Here we describe the detailed organization of the CX from posterior to anterior in the representative model brain.

The PB lies between two mushroom body (MB) calyces at the most posterior part of the brain. It is subdivided into 16 globular structures in a row denoted as glomerulus 1–8 from medial to lateral in each hemisphere (Figures 1B1 and 1C1), as previously reported (Hanesch et al., 1989). The central glomeruli incline slightly toward the anterior, giving the PB its unique handlebar shape (Figure 1A3). Anterior to the PB is the FB (Figures 1B2, 1C2, and 1C3). It can be subdivided into 48 subunits: six horizontal layers (a–f) stacked from dorsal to ventral and eight vertical columns denoted as 1–4 from medial to lateral in each hemisphere (Figure 1D1). Each FB layer is innervated by its own unique type of large field input F neurons (Figure S1A). Ventral to the FB is the spherical No, four paired neuropils (No_{1-4}), aligned symmetrically from dorsal to ventral along the midline (Figures 1B3, 1C7, and 1E). LTs are located laterally on both sides of the FB and defined as left LT (LT_L) and right LT (LT_R). Visual identification from the model brain indicated that each LT is composed of 80 microglomeruli characterized by their granular texture (Figures 1B4, 1C4, and 1E). The doughnut-shaped EB lies between the FB and the MB horizontal lobes and angled slightly upward so that the center canal faces anterodorsal (Figures 1B5, 1C4–1C6, and 1E). The EB can be further subdivided into eight concentric sectors from top to bottom in each hemisphere, and four horizontal doughnut-like concentric layers along the anterior-posterior axis, giving rise to a total of 64 subunits (Figure 1D2). Previously, four types of EB ring neurons (R1–R4) have been identified by means of Golgi impregnation (Hanesch et al., 1989). Using GFP-labeled *Gal4* expression, R4 was further subdivided into R4d and R4m (Renn et al., 1999). To avoid confusion with our nomenclature of vertical sectors, we renamed the EB substructures as center (C) ring containing R1 neurons, anterior (A) ring containing R2 and R3 neurons, and outer (O) ring containing R4d and R4m neurons. In addition, we have identified a posterior (P) ring based on its diameter in specific *Gal4* lines and its position relative to the five other types of ring neurons (Figure S1B). Finally, paired inferior dorsofrontal protocerebra (IDFPs) are located ventrolateral to the MB horizontal lobes and caudal to the antennal lobes (Chiang et al., 2011). The IDFP consists of a round body (RB), a dorsal spindle body (DSB), a ventral spindle body (VSB), and a large area of hammer-like hammer body (HB) (Figures 1B6 and 1C7; see also Figure S1C for the comparison of CX's nomenclature in different studies).

PB Neuron Classification

We analyzed CX connectivity of 662 single PB neurons labeled by MARCM: 136 neurons from eight selected *Gal4* lines with preferential expression in the PB (Figures S2A–S2C) and 526 neurons from the FlyCircuit database (http://www.flycircuit.tw) (Chiang et al., 2011). Using Dscam17.1::GFP (Wang et al., 2004) and Synaptotagmin::HA (Syt::HA) (Robinson et al., 2002) as markers of putative dendrites and axons, respectively, we classified the imaged PB neurons into 134 local neurons (LNs), 78 input projection neuron (PN^{in}), 424 output projection neurons (PN^{out}), and 26 neurons of undefined polarity (Tables S2A–S2D). Neurons in the same class innervate the same set of local processing units (LPUs). The entire PB is considered as one LPU, a brain region with its own population of LNs (Chiang et al., 2011), because several populations of LNs innervate exclusively within the unit and most LNs are large field neurons covering all or nearly all 16 glomeruli in both hemispheres. Neurons

(C) Volume models of CX subunits, including PB glomeruli (C1), FB columns (C2), FB layers (C3), LT glomeruli and EB sectors (C4), A and O rings of EB (C5), C and P rings of EB (C6), and No layers and DSB, VSB, RB, and HB of IDFP (C7).
(D) Spatial distribution of FB subunits (D1) and EB subunits (D2).
(E) Spatial relationships of CX subunits revealed by anterior views of a transparent CX model. Dotted line, brain middle line; scale bar represents 20 μm. Abbreviations are summarized in Table S1.
See also Figure S1 and Movie S1.

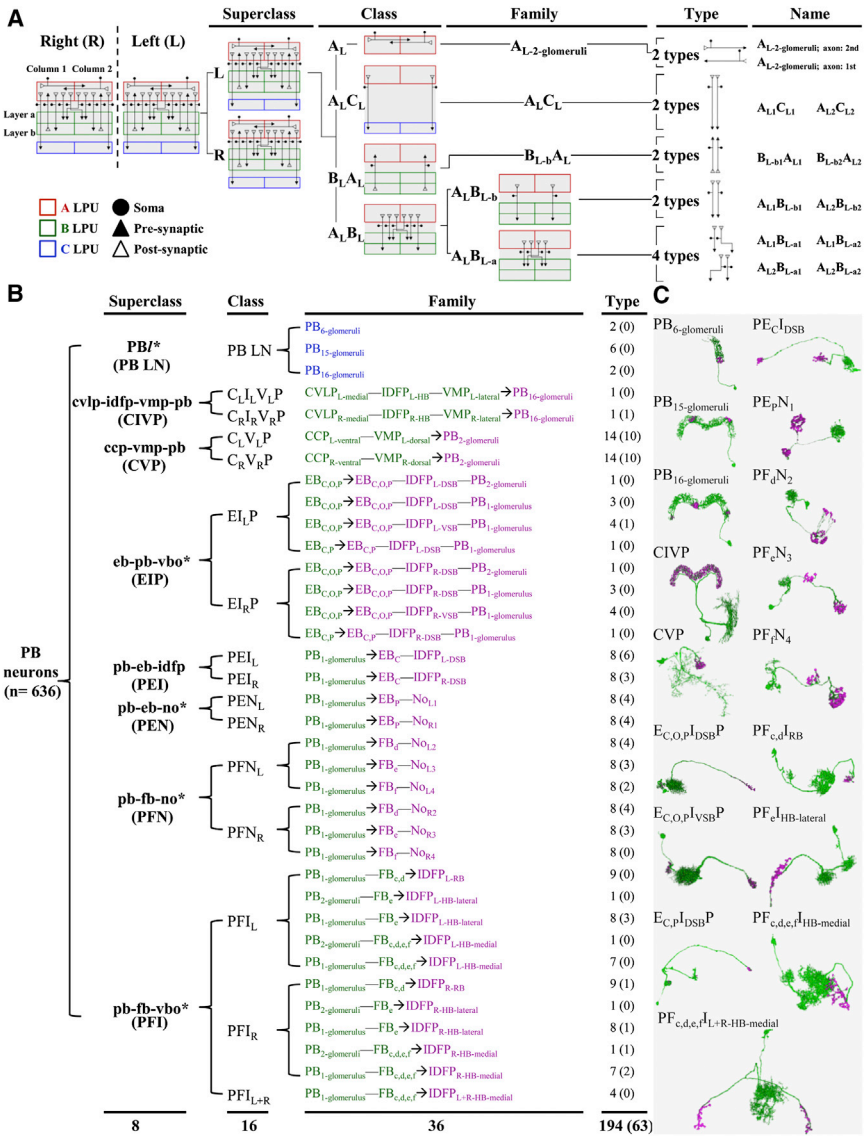

Figure 2. Classification and Nomenclature of PB Neurons

(A) Schematic diagrams of inferred principles of neuronal classification. The representative neurons in each hemisphere of the LPUs A, B, and C's belong to two superclasses. In the left hemisphere LPUs, there are 12 types of neurons belonging to five families forming 4 classes according to the LPU domains they innervate. Class 1 shows the arborization of two local neurons occupying an identical LPU, but their axons and dendrites innervate different columns. Class 2 demonstrates two projection neurons occupying two identical LPUs with their arborizations distributed in different columns. Eight distinctive types of projection neurons innervate two identical LPUs in class 3 and 4, which relay information in opposite directions. The information is transmitted from B to A in class 3, and A to B in class 4. Furthermore, neurons innervating distinctive LPU layers are categorized into different families in class 4. We defined neurons as identical whose axons and dendrites innervate the same LPU layers and columns. Neuron nomenclature is based on LPU innervation. The first character indicates the dendrite position and the last character indicates the axon position.

(B) Classification tree of 636 polarity-identified PB neurons. Arrows indicate the direction of information flow. The color key is as follows: magenta, axon; green, dendrite; blue, mixing of both. *Hanesch et al., 1989. Numbers in brackets are predicted cell types. See also Table S2.

(C) Representative images of PB neurons. The color key is as follows: magenta, axon terminals; green, neural expression pattern. For abbreviations, see Table S1.

See also Figure S2 and Movie S2.

innervating symmetric LPUs in the two hemispheres belong to the same superclass. Neurons innervating identical layers in the same LPUs are classified as being in the same family. Neurons with identical polarity and innervating the same LPU subunits are classified as the same type. Neurons of the same type with different neurotransmitter or gene expression are classified as different subtypes. This systematic nomenclature system resembles that used in taxonomy and provides an easy way for human to read and for machine to search. The structure of this naming principle is shown in Figure S2D. Representative images of each of 131 neuron types are illustrated in Figure S2E. Based on the foregoing criteria, we have morphologically classified 636 polarity-identified PB neurons (Table S2D) into 194 types (including predicted types) belonging to 36 families making up 16 classes, which in turn form eight superclasses (Figures 2B, 2C, anf S2E; Movie S2). Each of these PB neurons exhibits a remarkably stereotyped pattern of glomerular innervation and dendrite-axon putative connectivity (Tables S2D and S2E). This highly-ordered wiring principle has allowed us to predict an additional 63 types of PB neurons (see Figure 2B and Table S2E for the actual data and a list of predicted neuron types in each family). Note, however, that each PB glomerulus is likely to be innervated by more neurons than the number of cell types because isomorphic sister cells derived from two-cell clone are often seen (Figure S2F). Here we analyze the connectivity of all 194 types of PB neuron among CX subunits and aim to identify basic wiring principles governing information flow within the PB network.

A Comprehensive Local Wiring Diagram within the PB

LNs within an LPU may shape its output signals and modulate the input signals (Aonuma and Newland, 2002; Herman et al., 2002; Wilson, 2011). Systematic identification and characterization of LNs is a prerequisite for understanding how nervous systems process information (Olsen and Wilson, 2008). Based on differences in glomerular innervations, PB/ (PB LNs) are classified into three families: $PB_{6\text{-glomeruli}}$, $PB_{15\text{-glomeruli}}$, and

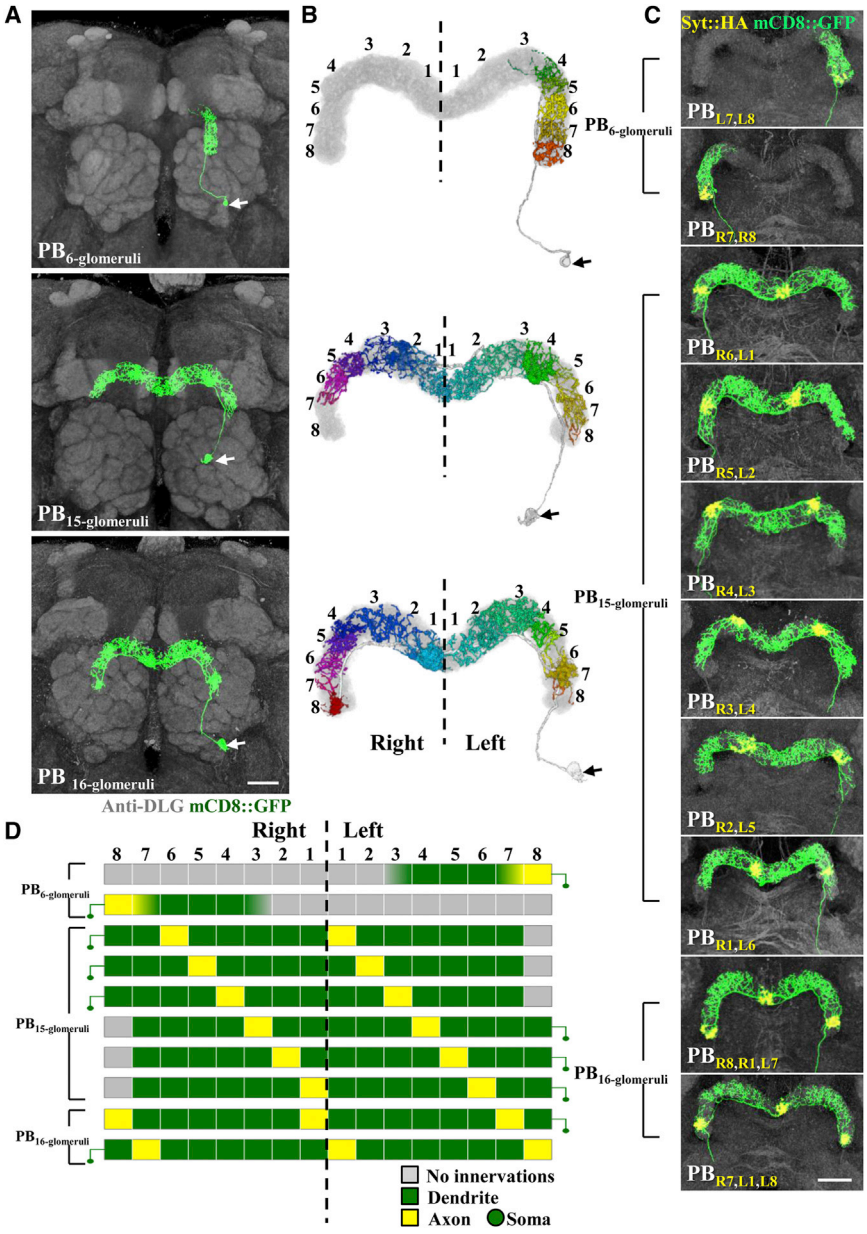

Figure 3. Connectivity Analysis for PB Local Neurons

(A) Three PB LN families. Representative fly brains containing GFP-labeled single LNs. Neuropils are counterstained with anti-DLG (gray).

(B) Reconstructions of LNs that innervate different PB glomeruli. PB glomeruli are color-coded as in Figure 1 and the PB neuropil background is shown in gray.

(C) Anterior projection images of 10 representative individual neurons. Color key: green, whole expression pattern of neuron; yellow, presynaptic terminals; gray, neuropil background.

(D) Wiring scheme of the LN system. Each line represents one LN in the PB (yellow, axon terminals; green, dendritic arborizations; gray, no innervation).

Arrows, cell bodies; dotted line, midline of the brain. Scale bar represents 20 μm. For abbreviations, see Table S1.

$PB_{16\text{-glomeruli}}$ (Figures 3A–3C and S2E1). The $PB_{6\text{-glomeruli}}$ family has two cell types: $PB_{R7,R8}$ and $PB_{L7,L8}$. $PB_{R7,R8}$ has ipsilateral innervations limited to glomeruli 3–8, with axon terminals distributed in the last two glomeruli (R7 and R8) in the right hemisphere. $PB_{L7,L8}$ is a mirror symmetrical neuron of $PB_{R7,R8}$ in the left hemisphere. The $PB_{15\text{-glomeruli}}$ family has 6 cell types: $PB_{L1,R6}$, $PB_{L2,R5}$, $PB_{L3,R4}$, $PB_{L4,R3}$, $PB_{L5,R2}$, and $PB_{L6,R1}$. They are characterized by innervation in 15 glomeruli; all but the contralateral terminal glomerulus. Each $PB_{15\text{-glomeruli}}$ neuron has axon terminals distributed in two glomeruli that are always spaced five glomeruli apart. The $PB_{16\text{-glomeruli}}$ family has two cell types: $PB_{R8,R1,L7}$ and $PB_{R7,L1,L8}$. They have innervations in all 16 glomeruli and axon terminals distributed in three glomeruli that are always spaced six glomeruli apart. Altogether, we have constructed a nearly comprehensive wiring diagram of LNs within the PB that reveals multiple stereotyped and direct patterns of local information flow (Figure 3D).

PB Inputs from Three Parallel Pathways

There are 48 types of PB input neurons belonging to 12 families that are divided into six classes based on their dendritic connections to LPUs outside of the PB (Figures 2 and 4). Henceforth, we use "→" to indicate the putative direction of information flow into and out of the PB, based on labeling of dendritic arbors (Dscam17.1::GFP-positive) and adjacent axon terminals (Syt::HA-positive) throughout this article.

The superclass of cvlp-idfp-vmp-pb (CIVP) neurons has only two symmetric types of wide-field neurons: $CVLP_{L\text{-}medial}$—$IDFP_{L\text{-}HB\text{-}lateral}$—$VMP_{L\text{-}lateral}$→PB and $CVLP_{R\text{-}medial}$—$IDFP_{R\text{-}HB\text{-}lateral}$—$VMP_{R\text{-}lateral}$→PB neurons (Figures 4A and S2E2). They have dendrites in the ipsilateral $CVLP_{medial}$, $IDFP_{HB\text{-}lateral}$, and $VMP_{lateral}$ and axons projecting along the PB handlebar to innervate all 16 PB glomeruli.

The superclass of ccp-vmp-pb (CVP) neurons has two classes; each has only one family containing 14 types (10 predicted) of isomorphic neurons (Figures 4B and S2E3). They have dendritic arbors in the ventral CCP and the dorsal VMP, and axon terminals in two consecutive PB glomeruli. We deduced three wiring principles for these neurons (Figure 4D; Movie S3): (1) each CVP neuron is paired with a symmetric neuron showing mirror-image wiring pattern in the opposite hemisphere (i.e., CCP_R—VMP_R→$PB_{R7,R8}$ and CCP_L—VMP_L→$PB_{L7,L8}$), (2) two consecutive PB glomeruli receive converged inputs from

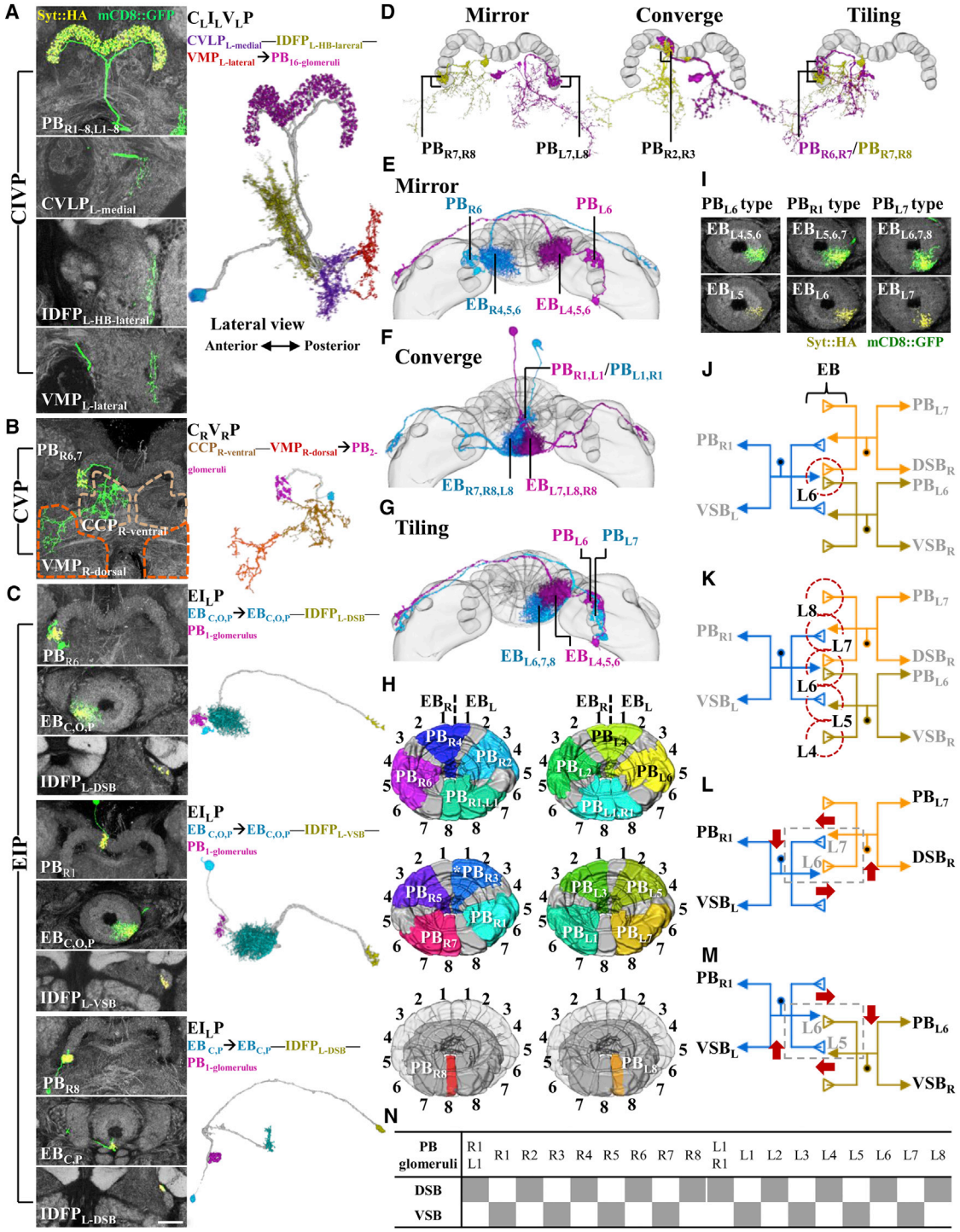

Figure 4. Connectivity Analysis for PB Input Neurons

(A–C) Three PB input PN superclasses. A representative neuron (green) with presynaptic terminals labeled by Syt::HA (yellow) is demonstrated for each of CIVP, CVP, and EIP superclasses. Neuropils are immunostained with anti-DLG (gray). Three-dimensional reconstructions of neurons innervating different neuropils are shown in different colors. The same color is used for fibers and their target neuropil. Blue, cell body.

(D) CVP neurons projected onto the 3D PB model (gray).

(E–G) $E_{C,O,P}I_{SB}P$ neurons projecting onto models of the PB, EB, and IDFP (gray).

(H) Spatial distribution of different types of EIP neurons in EB and their target PB glomeruli (colors). Asterisk, prediction.

(I) Three sets of representative confocal images showing single neurons labeled with GFP (green) and a presynaptic marker (yellow). The EB neuropil is counterstained with anti-DLG (gray).

(legend continued on next page)

opposite hemispheres (i.e., $CCP_R-VMP_R\rightarrow PB_{R2,R3}$ and $CCP_L-VMP_L\rightarrow PB_{R2,R3}$), and (3) two consecutive PB glomeruli have tiled inputs from the same hemisphere, overlapping by one glomerulus (i.e., $CCP_R-VMP_R\rightarrow PB_{R6,R7}$ and $CCP_R-VMP_R\rightarrow PB_{R7,R8}$).

The superclass of eb-pb-vbo (EIP) neurons has 18 neuronal types (1 predicted) belonging to eight families making up two classes, which in turn form one superclass. They have dendritic arbors in the EB and axon terminals in the EB, IDFP and PB (Figures 4C, S2E4, and S3A). Neurons in each family are distinguished by their patterns of dendritic innervation in the EB rings and/or the SB layers. Dendrites of $E_{C,O,P}I_{DSB}P$ and $E_{C,O,P}I_{VSB}P$ neurons innervate three consecutive EB sectors, whereas $E_{C,P}I_{DSB}P$ neurons are confined to one-half of one EB sector. Unlike CVP neurons, axons of most EIP neurons innervate only a single PB glomerulus. From the foregoing, we deduce four wiring principles of EB to PB connectivity: (1) each EIP neuron is paired with a symmetric neuron showing a mirror-image wiring pattern in the opposite hemisphere (i.e., $EB_{L4C,O,P;L6C,O,P}\rightarrow EB_{L5C,O,P}-IDFP_{R\text{-}DSB}-PB_{L6}$ and $EB_{R4C,O,P;R6C,O,P}\rightarrow EB_{R5C,O,P}-IDFP_{L\text{-}DSB}-PB_{R6}$) (Figure 4E; Movie S3), (2) two unique types of neuron receive converging inputs from two penultimate EB sectors to the central PB glomeruli (i.e., $EB_{L7C,O,P;R8C,O,P}\rightarrow EB_{L8C,O,P}-IDFP_{L\text{-}DSB}-PB_{R1,L1}$ and $EB_{R7C,O,P;L8C,O,P}\rightarrow EB_{R8C,O,P}-IDFP_{R\text{-}DSB}-PB_{R1,L1}$) (Figure 4F; Movie S3), (3) every two consecutive PB glomeruli show regular tiling innervation patterns, dendritic arbors overlapping one EB sector (i.e., $EB_{L4C,O,P;\ L6C,O,P}\rightarrow EB_{L5C,O,P}-IDFP_{R\text{-}DSB}-PB_{L6}$ and $EB_{L6C,O,P;L8C,O,P}\rightarrow EB_{L7C,O,P}-IDFP_{R\text{-}VSB}-PB_{L7}$) (Figure 4G; Movie S3), and (4) a single EB sector connects to three corresponding PB glomeruli (i.e., EB_{R1}: PB_{R4}, PB_{L4}, and PB_{L3}) (Figure 4H).

Axon terminals of EIP neurons are distributed not only in the IDFP and the PB, but also in specific EB sectors. Six wiring principles of EIP neurons connecting among EB sectors have been deduced: (1) axon terminals of a $E_{C,O,P}I_{SB}P$ neuron are confined to a single medial sector surrounded by dendrites in two neighboring EB sectors (Figure 4I); (2) each EB sector is innervated by axon terminals from one $E_{C,O,P}I_{SB}P$ neuron and by dendritic arbors from two other $E_{C,O,P}I_{SB}P$ neurons (e.g., the axon innervating EB_{L6} comes from $E_{C,O,P}I_{SB}P-PB_{R1}$ [blue] neuron, and the dendrites are from $E_{C,O,P}I_{SB}P-PB_{L6}$ [orange] and $-PB_{L7}$ [dark yellow] neurons) (Figure 4J); (3) information from five EB sectors converges into a single PB glomerulus by means of the regular axon-dendrite tiling connectivity of the EB (e.g., dendrites of $E_{C,O,P}I_{SB}P-PB_{R1}$ neuron in $EB_{\ L5,L7}$ connect to axons from $E_{C,O,P}I_{SB}P-PB_{L6}$ and $-PB_{L7}$ neurons) (Figure 4K), this type of connection enables $E_{C,O,P}I_{SB}P-PB_{R1}$ neuron receive not only information from $EB_{\ L5,L7}$, but also from $EB_{\ L4,L6,L8}$; (4) information in the EB shows antiparallel propagation through similar or different connections from $E_{C,O,P}I_{SB}P$ neuron families (i.e., counter-clockwise flow: $E_{C,O,P}I_{VSB}P\leftarrow\rightarrow E_{C,O,P}I_{DSB}P$ and clockwise flow: $E_{C,O,P}I_{VSB}P\leftarrow\rightarrow E_{C,O,P}I_{VSB}P$) (Figures 4L and 4M); (5) PB glomeruli spaced six apart from each other have connections to different neuron families, whereas glomeruli spaced five apart from each other have connections to similar neuron families (Figures 4L and 4M); and (6) a tiling loop of putative information flow among EB sectors is closed by a unique $E_{C,P}I_{DSB}P$ neuron that sends dendrites and axons to a single 8th sector of the C and P, but not O, rings between two hemispheres (i.e., $EB_{R8C,P}\rightarrow EB_{R8C,P}-IDFP_{L\text{-}DSB}-PB_{R8}$ and $EB_{L8C,P}\rightarrow EB_{L8C,P}-IDFP_{R\text{-}DSB}-PB_{L8}$) (Figure S2E4). In addition, EIP neurons also show a regular alternating pattern of innervation between PB glomeruli and $IDFP_{SB}$ domains (i.e., $PB_1-IDFP_{DSB/VSB}$, $PB_{3,5,7}-IDFP_{VSB}$, and $PB_{2,4,6,8}-IDFP_{DSB}$) (Figure 4N).

Together, the deduced wiring principles indicate a remarkable regularity of wiring pattern within and between the EB, PB, and $IDFP_{SB}$. Although juxtaposition of axons and dendrites in the same subunit is only a prerequisite for their synaptic connections, the deduced wiring principles have allowed us to formulate a model of stereotyped information reverberation among subunits within and between the EB and the PB (Figure S3B).

PB Outputs

There are 136 types of PB output neurons with dendritic arbors distributed in the PB belonging to 21 families forming nine classes, which in turn form four superclasses. Three superclasses (PEI, PEN, and PFN) have axon terminals in two other LPUs (EB/IDFP, EB/No, and FB/No, respectively) (Figure 5). The PFI superclass has additional dendritic arbors distributed in the FB and projects axon terminals only to the IDFP (Figure 6).

pb-eb-idfp (PEI) neurons link 1 PB glomerulus to two adjacent EB_C domains and terminate in the contralateral $IDFP_{DSB}$ (Figure 5A). Three wiring principles of PEI neurons are deduced (Figures 5D and S2E5; Movie S4): (1) each PEI neuron is paired with a symmetric neuron showing a mirror-image wiring pattern in the opposite hemisphere (i.e., $PB_{R6}\rightarrow EB_{R4C,R5C}-IDFP_{L\text{-}DSB}$ and $PB_{L6}\rightarrow EB_{L4C,L5C}-IDFP_{R\text{-}DSB}$), (2) PEI neurons innervating two PB glomeruli, spaced six glomeruli apart, converge onto two consecutive domains in the EB_C (i.e., $PB_{R1}\rightarrow EB_{L6C,L7C}-IDFP_{L\text{-}DSB}$ and $PB_{L7}\rightarrow EB_{L6C,L7C}-IDFP_{R\text{-}DSB}$), and (3) PEI neurons innervating two lateral-most PB glomeruli converge onto two consecutive center domains in the EB_C (i.e., $PB_{L8}\rightarrow EB_{L8C,R8C}-IDFP_{R\text{-}DSB}$ and $PB_{R8}\rightarrow EB_{CR8,L8C}-IDFP_{R\text{-}DSB}$). Based on the foregoing principles, we have constructed a PEI wiring model in which outputs from two selected PB glomeruli converge onto two consecutive sectors in the EB_C (Figure 5E).

pb-eb-no (PEN) neurons link 1 PB glomerulus to two adjacent EB_P domains and terminate in contralateral No_1 (Figure 5B). Three wiring principles of PEN neurons are deduced (Figures 5F and S2E6; Movie S4): (1) each PEN neuron is paired with a symmetric neuron showing mirror symmetrical wiring pattern in the opposite hemisphere (i.e., $PB_{R6}\rightarrow EB_{R2P,R3P}-No_{L1}$ and $PB_{L6}\rightarrow EB_{L2P,L3P}-No_{R1}$), (2) two adjacent EB sectors receive

(J–M) Proposed connectivity scheme of $E_{C,O,P}I_{SB}P$ neurons. Filled arrow, axon; open arrow, dendrite; spheroid, cell body. Colors were randomly assigned to individual neurons.

(N) Innervation patterns between PB glomeruli and $IDFP_{SB}$ domains. Gray squares indicate single EIP neuron's arbors into specific PB glomeruli and $IDFP_{SB}$ domains.

Scale bars represent 20 μm. For abbreviations, see Table S1. See also Figure S3 and Movie S3.

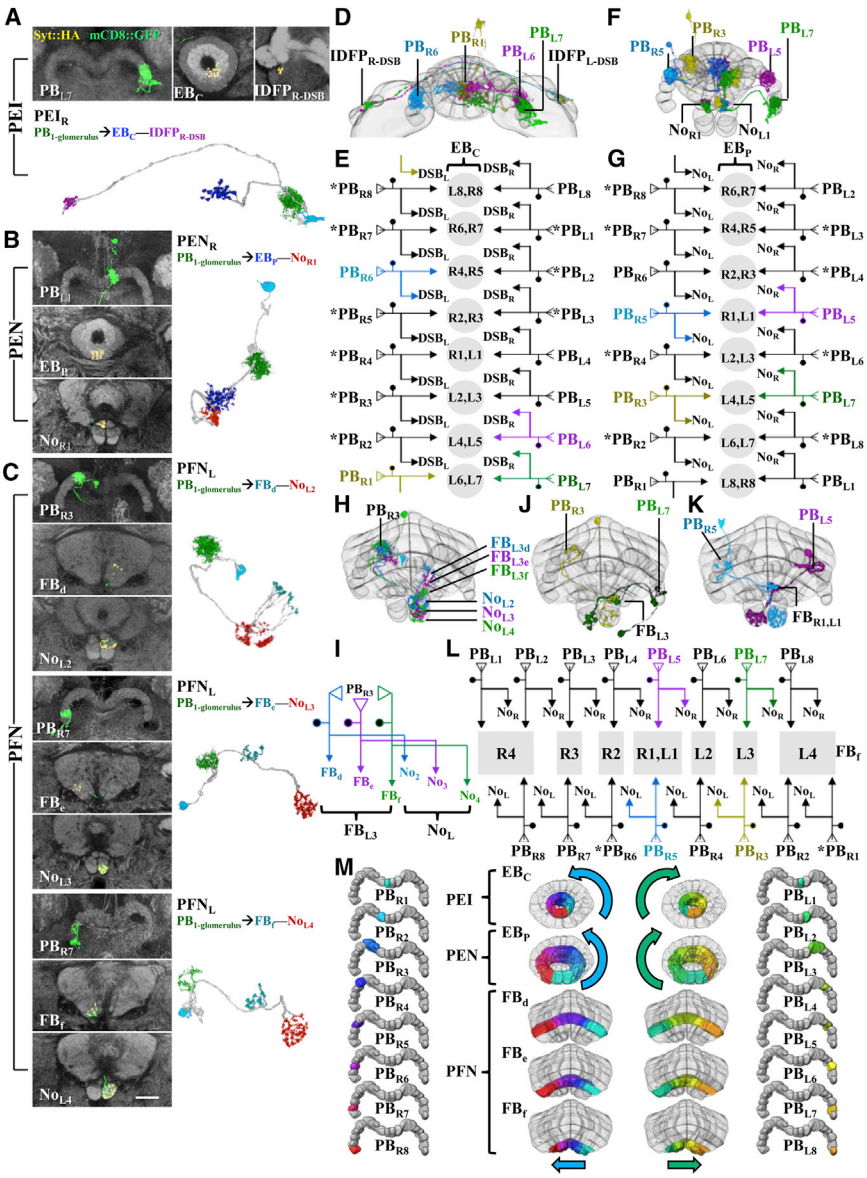

Figure 5. Connectivity Analysis for PB Output Neurons PEI, PEN, and PFN

(A–C) Three PB output PN superclasses. A representative neuron (green) with presynaptic terminals labeled by Syt::HA (yellow) is demonstrated for each of PEI, PEN, and PFN superclasses. Neuropils are immunostained with anti-DLG (gray). Three-dimensional reconstructions of neurons innervating different neuropils are shown in different colors. The same color is used for fibers and their target neuropil. Blue, cell body.

(D) Spatial distributions of four representative PEI neurons.

(E) Proposed connectivity scheme of PEI circuits. Neurons are color-coded as in (D).

(F) Spatial distributions of four representative PEN neurons.

(G) Proposed connectivity scheme of PEN circuits. Neurons are color-coded as in (F).

(H) Spatial distributions of representative PFN neurons from three different families.

(I) Proposed connectivity scheme of PFN circuits illustrating divergence of three neurons from different PFN families. These PFN neurons project from one PB glomerulus (PB_{R3}) to three different FB layers ($FB_{L2,d,e,f}$) and three different No layers ($No_{L2,3,4}$). Neurons are color-coded as in (H).

(J and K) Spatial distributions of four representative PFN neurons of the same family.

(L) Proposed connectivity scheme of PFN circuits illustrating convergence of paired PFN neurons from different PB glomeruli to the same FB subunit. Neurons are color-coded as in (J) and (K). Asterisk, predicted neuron; filled triangle, axon; open triangle, dendrite; spheroid, cell body.

(M) Spatial distributions of PEI, PEN, and PFN dendritic arborizations in different PB glomeruli and their corresponding axon terminals in different $EB_{C,P}$ and $FB_{d,e,f}$ subunits. Domains of $EB_{C,P}$, $FB_{d,e,f}$, and PB are colored according to neuron types.

Arrows indicate innervation sequence in EB or FB. Scale bars represent 20 μm. For abbreviations, see Table S1. See also Figure S4 and Movie S4.

convergent inputs from two symmetric PB glomeruli (i.e., $PB_{R5}\rightarrow EB_{R1P,L1P}-No_{L1}$ and $PB_{L5}\rightarrow EB_{R1P,L1P}-No_{R1}$), and (3) two adjacent EB sectors receive convergent common inputs from two nonsymmetric PB glomeruli spaced eight glomeruli apart (i.e., $PB_{R3}\rightarrow EB_{L4P,L5P}-No_{L1}$ and $PB_{L7}\rightarrow EB_{L4P,L5P}-No_{R1}$). Based on the foregoing principles, we have constructed a PEN wiring model in which outputs from two selected PB glomeruli converge onto two consecutive sectors in the EB_P (Figure 5G).

pb-fb-no (PFN) neurons are equivalent to the set of isomorphic neurons forming the vertical fiber system (Hanesch et al., 1989), in which each neuron links one PB glomerulus to one FB layer and terminate in one contralateral No (Figure 5C). Nevertheless, we found that PFN fibers exhibit a crossing-over arrangement between the PB and the FB (Figure S4A). Six wiring principles of PFN neurons have been deduced: (1) each PFN neuron is paired with a symmetric neuron showing mirror symmetrical wiring pattern in the opposite hemisphere (i.e., $PB_{L1}\rightarrow FB_{R4d}-No_{R2}$ and $PB_{R1}\rightarrow FB_{L4d}-No_{L2}$) (Figure S2E7), (2) two adjacent FB sectors receive convergent inputs from two symmetrical PB glomeruli (i.e., $PB_{R5}\rightarrow FB_{L1d,R1d}-No_{L2}$ and $PB_{L5}\rightarrow FB_{L1d,R1d}-No_{R2}$) (Figure S2E7), (3) each PB glomerulus sends divergent outputs to three consecutive domains of the same column in the FB and three consecutive domains in the contralateral No (i.e., $PB_{R3}\rightarrow FB_{L3d}-No_{L2}$, $PB_{R3}\rightarrow FB_{L3e}-No_{L3}$, and $PB_{R3}\rightarrow FB_{L3f}-No_{L4}$) (Figures 5H and 5I; Movie S4), (4) each FB domain receives convergent inputs from two nonsymmetrical PB glomeruli spaced eight glomeruli apart (i.e., $PB_{R3}\rightarrow FB_{L3f}-No_{L4}$ and $PB_{L7}\rightarrow FB_{L3f}-No_{R4}$) (Figure 5J; Movie S4), (6) two center FB domains in each of three FB bottom layers ($FB_{R1d,L1d}$, $FB_{R1e,L1e}$, $FB_{R1f,L1f}$) receive convergent inputs from two symmetric PB_5 glomeruli (i.e., $PB_{R5}\rightarrow FB_{L1f,R1f}-No_{L4}$ and

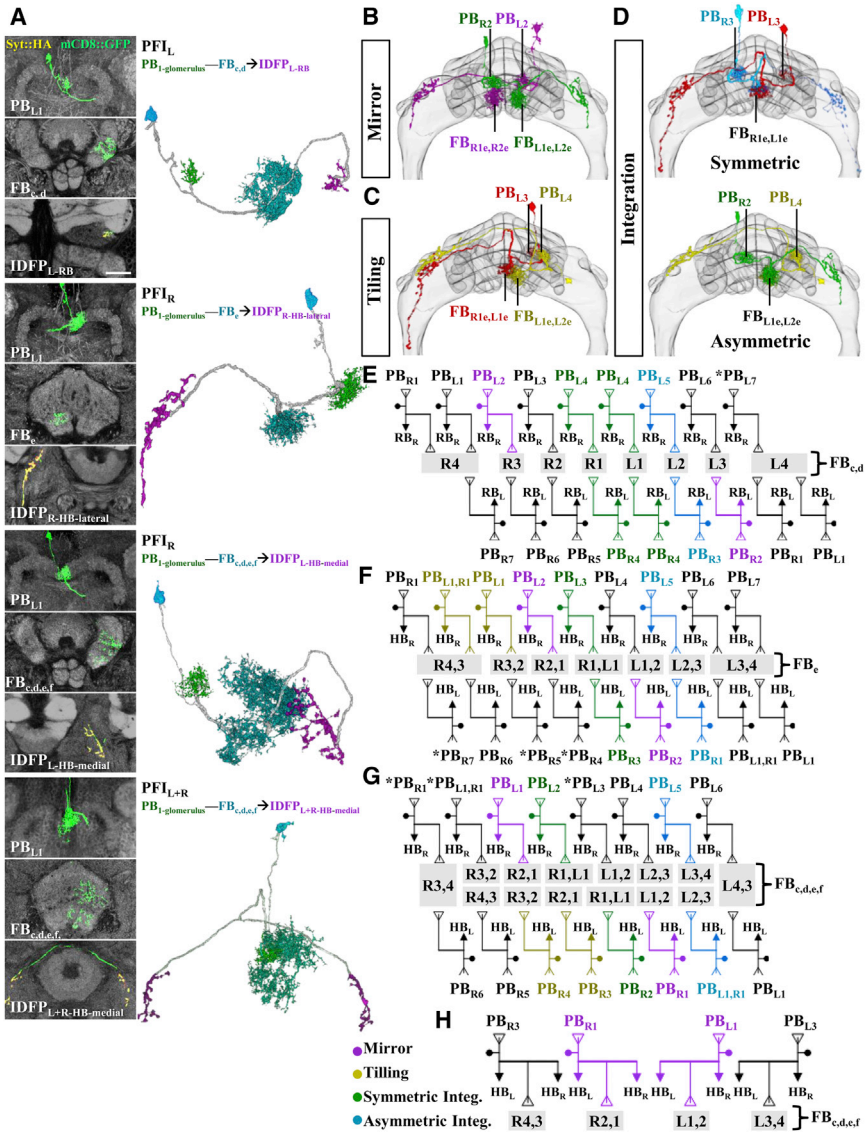

Figure 6. Connectivity Analysis for PB Output PFI Neurons

(A) Four representative PFI neurons (green) with presynaptic terminals labeled by Syt::HA (yellow). Neuropils are immunostained with anti-DLG (gray). Three-dimensional reconstructions of neuron with colored arborizations indicating innervation in different neuropils (the same color). Blue, cell body.

(B–D) Spatial distribution of representative PFI neurons illustrating mirror (B), tiling (C), and symmetric and asymmetric (D) innervation patterns. Each color represents a specific type of PFI neuron.

(E–H) Proposed connectivity schemes for $PF_{c,d}I_{RB}$ (E), $PF_eI_{HB\text{-}lateral}$ (F), $PF_{c,d,e,f}I_{HB\text{-}medial}$ (G), and $PF_{c,d,e,f}I_{L+R\text{-}HB\text{-}medial}$ (H) neurons, respectively.

Asterisk, prediction; filled triangle, axon; open triangle, dendrite; spheroid, cell body. Scale bar represents20 μm. For abbreviations, see Table S1. See also Figure S5 and Movie S5.

pb-fb-idfp (PFI) neurons are equivalent to the set of isomorphic neurons forming the horizontal fiber system (Hanesch et al., 1989), in which each neuron receives inputs from both PB and FB, and projects outputs to IDFP through four different sets of isomorphic PFI neurons (Figures 6A and S5A). Several PFI wiring principles have been deduced: (1) PB_8 glomerulus is the one glomerulus not innervated by PFI neurons, based on expression patterns in the *VT27015*, *VT16998*, and *VT1979 Gal4* lines (Figures S2E8 and S5B), (2) each of the glomeruli from PB_1 to PB_7 has its own unique PFI neuron combining information from various FB domains and terminating in RB or HB in one or both sides of the IDFP (Figure S5C), (3) each set of PFI neurons is paired with a symmetric neuron showing a mirror-image wiring pattern in the opposite hemisphere (i.e., $PB_{L2}-FB_{R1e,R2e}\rightarrow IDFP_{R\text{-}HB\text{-}lateral}$ and $PB_{R2}-FB_{L1e,L2e}\rightarrow IDFP_{L\text{-}HB\text{-}lateral}$) (Figures 6B and 6E–6H; Movie S5), (4) two consecutive PB glomeruli show regular tiling innervation patterns, dendritic arbors overlapping on one FB column (i.e., $PB_{L3}-FB_{R1e,L1e}\rightarrow IDFP_{R\text{-}HB\text{-}lateral}$ and $PB_{L4}-FB_{L1e,L2e}\rightarrow IDFP_{R\text{-}HB\text{-}lateral}$) (Figures 6C, 6F, and 6G; Movie S5), and (5) outputs from two selected PB glomeruli spaced by a fixed number of glomeruli symmetric or asymmetric integrate with outputs from the same FB domain(s) to the IDFP (i.e., symmetric: $PB_{L3}-FB_{R1e,L1e}\rightarrow IDFP_{R\text{-}HB\text{-}lateral}$ and $PB_{R3}-FB_{R1e,L1e}\rightarrow IDFP_{L\text{-}HB\text{-}lateral}$, asymmetric: $PB_{L4}-FB_{L1e,L2e}\rightarrow IDFP_{R\text{-}HB\text{-}lateral}$ and $PB_{R2}-FB_{L1e,L2e}\rightarrow IDFP_{L\text{-}HB\text{-}lateral}$) (Figures 6D and 6E–6G; Movie S5). Based on the foregoing principles we have constructed a PFI wiring model of information flow among the PB, FB, and IDFP (Figures 6E–6H).

$PB_{L5}\rightarrow FB_{R1f,\ L1f}-No_{R4}$) (Figure 5K; Movie S4), and (6) the two lateral most FB domains in each of three FB bottom layers (FB_{R4d}, FB_{R4e}, FB_{R4f}, FB_{L4d}, FB_{L4e}, or FB_{L4f}) receive convergent inputs from three pairs of PB glomeruli (i.e., PB_{L1}/ PB_{R1}, PB_{L2}/ PB_{R2}, PB_{L8}/ PB_{R8}) (Figure S2E7). Based on the foregoing principles, we have constructed a PFN wiring model of information flow among the PB, FB, and No (Figures 5L and S4B).

Our models of PEI, PEN, and PFN wiring reveal that these PB output neurons share a common feature: sequential PB_R glomeruli link to sequential $EB_{C,P}$ sectors in a counter-clockwise manner, whereas sequential PB_L glomeruli link to sequential $EB_{C,P}$ sectors in a clockwise manner. Similarly, PB_R glomeruli link to $FB_{d,e,f}$ domains from left to right whereas PB_L glomeruli link to $FB_{d,e,f}$ domains from right to left. Together, signals from spaced pairs of PB glomeruli converge onto specific EB sectors and FB domains in a highly-ordered, progressive sequence (Figure 5M).

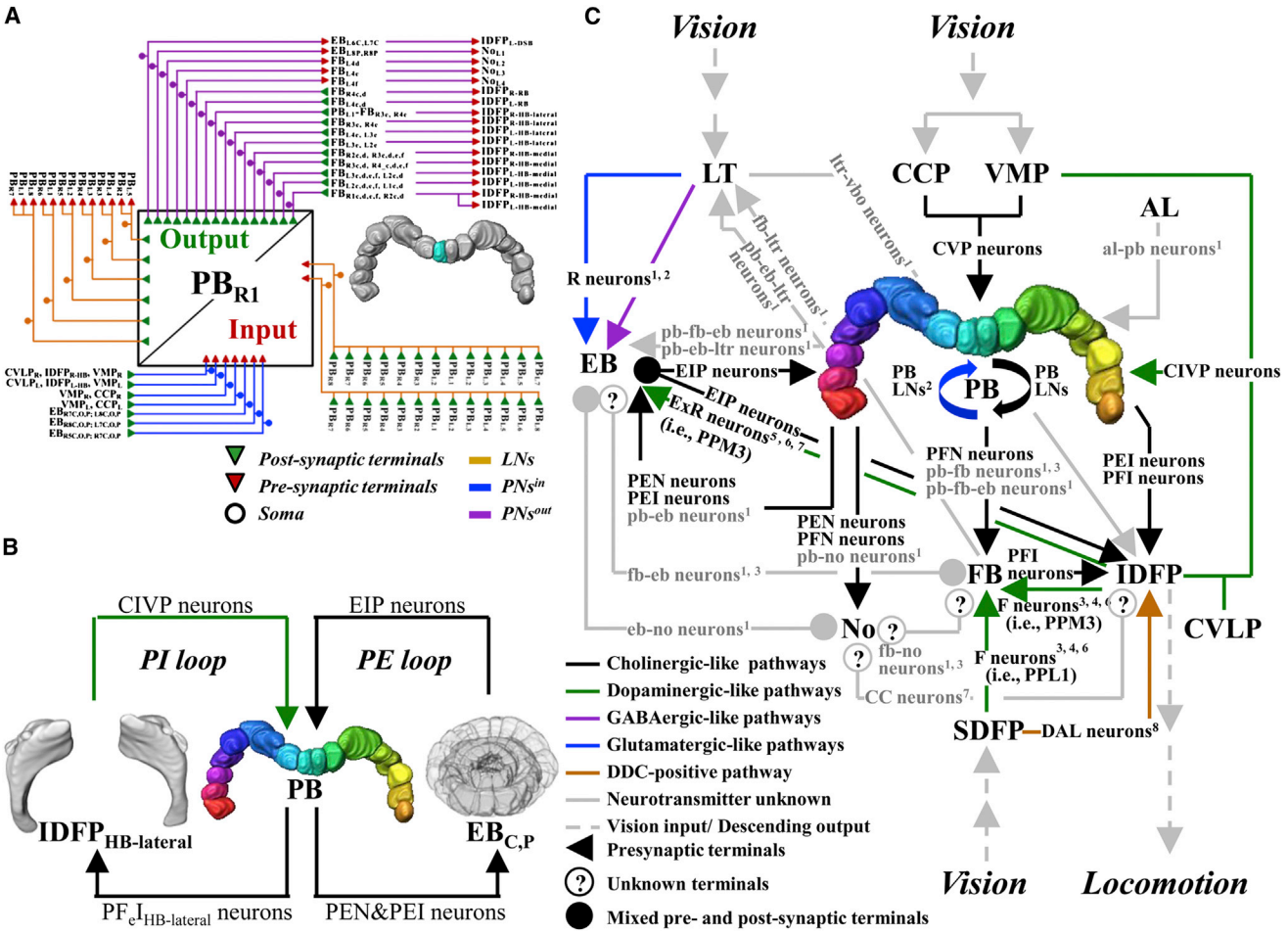

Figure 7. Wiring Diagram of PB Network

(A) Generalized anatomy of a PB glomerulus, using PB_{R1} as an example. Different types of input and output neurons innervate the glomerulus, demonstrating the multiple possibilities of connectivity. PN^{in} neurons are shown in blue, local neurons confined to PB in brown, and PN^{out} neurons in magenta. Arrowheads represent dendritic arborizations (green) and axon terminals (red), respectively. Convergent and divergent connectivity is shown.

(B) Two proposed reverberation loops between PB/IDFP (PI loop) and PB/EB (PE loop), with synapses in PB, $IDFP_{HB}$, and $EB_{C,P}$ respectively.

(C) A model of directed information flow in the CX wiring networks. Visual inputs to the CX are presumably relayed via LT, CCP, VMP, SDFP and IDFP. CX presumably controls locomotion through IDFP. [1]Hanesch et al., 1989; [2]Daniels et al., 2008; [3]Young and Armstrong, 2010b; [4]Liu et al., 2012; [5]Kong et al., 2010; [6]Mao and Davis, 2009; [7]Yu et al., 2009; [8]Chen et al., 2012. For abbreviations, see Table S1.

See also Figure S6 and Movie S6.

Models of Information Flow

When the results of the foregoing analysis are integrated, they permit us to construct a comprehensive wiring diagram of PB circuitry indicating a pattern of complex but unique local connectivity for each PB glomerulus (Movie S6). We found that each of the eight PB glomeruli in the same hemisphere is uniquely innervated by a different number of cell types, suggesting that there is functional diversity among different glomeruli (Figure S6A). For example, axon terminals derived from at least nine cell types (two types of LNs and seven types of PB input PNs) and dendritic arbors derived from at least 22 cell types (six types of LNs and 16 types of PB output PNs) intersect in the PB_{R1} or PB_{L1} glomerulus (Figure 7A). Other glomeruli are innervated by significantly fewer cell types (Figure S6A). Overall, PB local circuits exhibit an unexpected neural complexity, despite showing a high degree of stereotypical connections among its 16 glomeruli. Each glomerulus shows multiple instances of divergence and convergence of information, likely to be important for carrying out complex synaptic computations. Such complexity should translate into variability and versatility in the functions of PNs^{in}, LNs, and PNs^{out} in the PB.

Based on the intersection between PN^{in} dendrites and PN^{out} axons outside of the PB (Figures S2C), we propose two reverberating information loops in the CX relaying PB information (Figure 7B). The first loop is between the PB and $EB_{C,P}$ (termed the PE loop). Immunohistochemical labeling indicates that PB output PEN (Figure S6B6) and PEI (Figure S6B8) and input EIP (Figure S6B5) are both cholinergic. The second loop is between the PB and $IDFP_{HB}$ (termed the PI loop). PB output $PF_eI_{HB\text{-}lateral}$ neurons are cholinergic (Figures S6B7 and S6B8) and PB input

CIVP neurons are dopaminergic (Figure S6B3). Notably, immunohistochemical labeling did not reveal any GABA-immunopositive neurons in the eight selected *Gal4* lines, including PB LNs (Figures S6B1 and S6B2) and CVP neurons (Figure S6B4).

DISCUSSION

The picture of PB wiring that our study presents is that of a highly structured region characterized by recursive and sequentially iterative patterns of input, output, and cross connection. We systematically imaged 662 single PB neurons that were classified into 131 distinct PB neuron types, including five superclasses identified previously (Hanesch et al., 1989), three superclasses (i.e., CIVP, CVP, and PEI neurons), and numerous cell types. Connectivity analysis of this comprehensive list of PB neurons revealed several fundamental wiring principles linking substructures within the CX: the mirror, convergence, divergence, tiling, reverberation, and parallel signal propagation of circuit properties beyond that described previously in any insect. This organization, in conjunction with the key position that the CX occupies in the fly brain's overall scheme of connectivity, suggests that the PB performs important computational tasks in the fly brain, and may even contain one of the few topographical maps to be found outside of the primary sensory regions of the optic and olfactory lobes. This layout of PB neuronal circuitry will be useful as a resource to *Drosophila* neurobiologists who are working to reveal functional circuits that control specific behaviors. Nevertheless, this PB wiring map is still incomplete for missing at least 12 neuron types of undefined polarity (Figure S2E9) and several Golgi-labeled neurons identified previously (Figure S6C).

Terminology

Because the new science of connectomics that is emerging depends so completely on the ability to assign standard positional coordinates to large numbers of neurons and demands that they be machine searchable, we have had to modify and expand upon previous anatomical names to some extent. Where possible, we have retained earlier designations, and we also provide a comparison table to show where previous names fit into our current scheme (Table S1). A similar process of machine searchable streamlining and modification became necessary as gene lists became whole-genome systems in the early days of genomics. They do not detract from the importance of what came before. Instead they allow it to become more versatile and amenable to bioinformatic analysis. As in biological taxonomy, we believe that systematic classification of thousands of brain neurons is crucial for the understanding of brain function and fundamentally important to the study of neuronal diversity and conservation. In our view, a neuron type should be defined not only by its morphology but also by its content and connectivity.

Furthermore, we have now based the classifications of brain regions and substructures on the statistical criterion of the clustering of internally connected neurons ("Local Processing Units" definition of Chiang et al. [2011]), and we have expanded the number of neuron types over those reported previously, based on a finer grained definition of the spatial distribution of their putative dendrites and axons. Thus, isomorphic neurons innervating different LPU subunits, conventionally considered as the same type of neuron (Hanesch et al., 1989; Young and Armstrong, 2010b), are now considered as different type of neurons in the same family (Figure 2A). Although we find confirmation of much of what has been reported before (Hanesch et al., 1989; Renn et al., 1999; Young and Armstrong, 2010a, 2010b), we have also been able to expand upon it and catalog identified individual neuron types systematically in a model brain with standardized coordinates, along with concomitant classification of their connection patterns.

The Architecture of *Drosophila* CX

Golgi impregnation and nc82 immunostaining coupled with *Gal4* expression patterns revealed 16 glomeruli in PB, eight or 16 columns for each of six or eight horizontal layers in FB, 16 sectors for each of two EB subregions, and four or six domains in No (Hanesch et al., 1989; Renn et al., 1999; Young and Armstrong, 2010b; see also Figure S1C). Using DLG immunostaining with high-resolution confocal imaging, we confirmed these previous findings and generated volume models for each CX substructure accordingly (Figure 1B). The generated CX volume model allows us to compile 131 PB neuron types into a common framework and then re-examine CX architecture in detail. The architecture of 16 PB glomeruli is further confirmed by a comprehensive local wiring diagram with stereotyped innervation patterns and domain specific connections of PNs^{in} and PNs^{out} (Figure 7A).

For FB, our data support the architecture of eight columns for each of six horizontal layers (Hanesch et al., 1989). First, six different types of F neuron innervate respectively each of the six horizontal layers (Figure S1A). Second, PFN and PFI neurons exhibit either uni- or duocolumnar innervations (Figure S2E). However, whether FB column/layers may be further subdivided into more domains requires further study, because most FB neurons (i.e., fb-eb and pontine neurons) were not included in the current study (see also Young and Armstrong, 2010b).

For EB, we archived six different neuron types obtained from specific *Gal4* lines into a common volume framework and thus presented a nonoverlapping spatial map with distinct innervation patterns (Figure S1B). It is possible that the fly EB is homologous to the locust CBL that has six layers (Müller et al., 1997). Meanwhile, innervation patterns of EIP, PEI, and PEN neurons support the previous anatomical definition of 16 sectors in each EB ring.

A four-tiered layer arrangement in No was revealed by both DLG immunostaining and presynaptic innervation from different sets of PEN and PFN neurons targeting specific No layers (Figures 5B and 5C). This layer-specific No targeting has been previously shown by fb-no neurons (Young and Armstrong, 2010b) and CPU4 and CL2 neurons in the locust (Heinze and Homberg, 2008).

We also generated volume models for two CX accessory regions (i.e., LT and IDFP). We did not find any neuron linking directly between PB and LT. IDFP (Chiang et al., 2011) is a large ventrolateral CX accessory region originally termed VBO (Hanesch et al., 1989; Young and Armstrong, 2010b) or LAL (Heinze and Homberg, 2008; Heinze and Reppert, 2012; Williams and Boyan, 2008) based on morphological boundary. However, unlike other neuropilar regions, morphological boundaries defined by either nc82 or DLG immunostaining were ambiguous.

By coalescing populations of LNs, we have recently refined the morphological boundary of the region and termed it IDFP (Chiang et al., 2011). A freely accessible online database (http://www.flycircuit.tw) has been established to allow cross-lab examination of spatial relationships between individual neurons and neuropils. Because of different boundary definition and consistent with the database for cross-lab examination, we adopted IDFP to represent the region in the current study. Interestingly, different PB neurons (i.e., CIVP, EIP, PEI, and PFI neurons) terminate at specific IDFP sub-regions (i.e., RB, VSB, DSB, and HB) suggesting functional diversity for these IDFP subregions. The existence of large field vbo-vbo neurons (Young and Armstrong, 2010b) connecting to both IDFPs suggests that CX information could be exchanged between two hemispheres before initiating locomotion.

Information Flow and Connectivity

The dendrite-axon polarity of more than 12 morphologically distinct types of *Drosophila* PB neurons has been previously predicted from Golgi staining and *Gal4* labeling (Hanesch et al., 1989; Young and Armstrong, 2010b). Here, using polarity markers, we confirmed innervation patterns and polarity for at least five superclasses of PB neurons, even for the EIP neurons with mixed dendritic and axonal terminals in the EB (Hanesch et al., 1989) (Figure S6C). Although three superclasses of PB neurons were identified, the constructed PB wiring map is still incomplete because several Golgi-labeled PB neurons were not included (Figure S6C). Notably, the deduced information flow is entirely based on the assumption that the distribution of Dscam17.1::GFP and Syt::HA might be correlated with the position of post- and presynaptic terminals, respectively (Wang et al., 2004; see Nicolai et al., 2010 for some exceptions). Thus, structural connectivity at the EM level and/or functional connectivity with electrophysiology or calcium imaging will be necessary to decisively determine the direction of information flow.

Single neuron analysis together with previous results (Figure S6D) has allowed us to formulate a wiring model of directed information flow in the CX circuit (Figure 7C). The model predicts that visual information arrives in the *Drosophila* CX via four major pathways: (1) an excitatory pathway formed by cholinergic CVP neurons that relay CCP and VMP information to specific PB glomeruli, (2) a dopaminergic pathway formed by large field F neurons that relay SDFP information to specific FB layer, (3) an inhibitory pathway formed by GABAergic large field ring neurons that relay LT information to specific EB subregion, and (4) a dopaminergic pathway formed by large field CIVP neurons that relay IDFP signals to the entire PB. Meanwhile, at least four different wiring properties suggesting strategies of processing signals in the CX were observed: (1) the converging circuitries (i.e., EB, IDFP, PB, SDFP→FB), (2) the diverging circuitries (i.e., EB→FB, IDFP, No, PB), (3) the bidirectional circuitries (i.e., EB←→IDFP and FB←→IDFP), and (4) reverberation loops (i.e., PI and PE loops, see also Figure 7B).

In FB, PFI neurons presumably integrate PB, SDFP, EB, No, and IDFP information and then project or feedback to IDFP by F, PFN, pb-fb, fb-eb, and fb-no neurons (Hanesch et al., 1989; Young and Armstrong, 2010b). It is already known that F neurons play a role in visual pattern memory and promote wakefulness (Li et al., 2009; Liu et al., 2006; Liu et al., 2012; Mao and Davis, 2009; Wang et al., 2008). Thus, as the target region of PFI neurons, the IDFP receives various kinds of information to control motor activity (Strauss, 2002). In addition, results of immunohistochemical labeling indicate that most PB neurons, including projection and local neurons, release excitatory signals (Figure S6B). Because the excitatory network is prone to runaway excitation, sustained firing must involve recruitment of inhibitory or modulatory neurons (Wilson, 2011). We propose that the GABAergic ring neurons with dense presynaptic terminals occurring in each EB vertical sector (Hanesch et al., 1989), and dopaminergic CIVP neurons with axon terminals in every PB glomeruli, can help the network satisfy the competing demands of information transmission and network stability (Durstewitz et al., 2000).

Thus, CX acts as a joint operation center using complex neuromodulation systems along with information integration and reverberation to control vision-based locomotion. With an extensive list of CX-specific *Gal4* drivers for activity manipulation (Figure S6D), functional and behavioral experiments will eventually unwrap the mystery of visual information processing in the complex CX circuits.

Functional Implications

In the locust, PB neurons have been shown to be involved in polarized light processing (Heinze et al., 2009; Heinze and Homberg, 2008, 2009). Similar superclasses of PB neurons exist in both the locust and the fly (Figure S6C). Comparison of the innervation, polarity, and heterolateral connectivity patterns of the EIP, PEI, PEN, PFN, and PFI neurons in the fly indicate that they are highly similar to the CL1a, CL1b/d, CL2, CPU4, and CPU1/2 neurons in the locust. Structural similarity suggests that PB neuronal functions present in the locust are likely also present in the fly.

In the locust, polarized light information from the anterior optic tubercle is preprocessed by neurons of the lower division of the central body (homologous to the EB) and conveyed to the PB (Homberg et al., 2011). The current study confirms this in *Drosophila*: directional clues encoded in the EB are maintained in the PB and further represented in the subunits of FB, EB, No, and IDFP regions (Figures 4, 5, and 6). In locusts, most PB neurons respond at least weakly to changes in E-vector orientation during zenithal stimulation with a rotating polarization filter (Figure S6C) (Heinze et al., 2009; Heinze and Homberg, 2007, 2009; Vitzthum et al., 2002). It has been suggested that the PB serves as an internal compass providing direct information on the azimuth of the sun over a 180° arc (Homberg et al., 2011). Behavioral experiments have shown that the fly can detect linearly polarized light from the sky or from shiny surfaces to help maintaining a steady course (Weir and Dickinson, 2012; Wernet et al., 2012). The sophisticated neural map presented in this study provides possible insight into understanding how the azimuthal map representation in the PB elicits appropriate behavior responses.

Possible Resemblance to Basal Ganglia

Aside from the similarities of the PB among various arthropod species, there are hints of a resemblance to the more distantly related mammalian basal ganglia, perhaps for the CX as a whole,

as has been suggested previously (Wessnitzer and Webb, 2006). The regions share the following characteristics: (1) motor control and sequencing (Strauss, 2002; Wessnitzer and Webb, 2006), (2) modulation of anticipation and visual attention (Foley et al., 2012; Triphan et al., 2010; van Swinderen and Greenspan, 2003), (3) substantial dopaminergic innervation (Chiang et al., 2011; Wessnitzer and Webb, 2006), (4) a recurrent anatomical loop motif (Figure 7B) (Wessnitzer and Webb, 2006), and (5) expression of a similar set of cell fate determination genes in their embryonic precursors (see following discussion). Since the inception of comparative neuroanatomy, it has been generally assumed that there is a complete lack of homology between invertebrate and vertebrate nervous systems (Sandeman, 1999; Strausfeld and Seyfarth, 2008), and that any relevance of invertebrates to vertebrates would be at the abstract level of functional strategies, rather than conserved mechanisms. This assumption has been brought into question by the finding of substantially conserved patterns of cell fate determination gene expression between invertebrate and vertebrate embryonic nervous systems (de Velasco et al., 2007; Tessmar-Raible et al., 2007; Tomer et al., 2010). Although impressive, this conservation does not necessitate any conservation of adult brain function, but evidence for one example, the similarity of the insect pars intercerebralis to the vertebrate hypothalamus, has been found. In addition to the existing evidence for similarity in embryonic gene expression (de Velasco et al., 2007), the corresponding structures use the same EGFR signaling system for sleep/wake control (Foltenyi et al., 2007), and the same cells in both organisms express and utilize insulin-like peptide (de Velasco et al., 2007; Dun et al., 2006).

Turning to the CX, its embryonic precursors are found among the type II neuroblasts (Bayraktar et al., 2010), in the dorsal-medial-posterior region of the anlagen (Izergina et al., 2009), and the basal ganglia precursors are in the subpallium (Flames et al., 2007). Of the genes involved in cell fate, regionalization, and specification that are conserved between flies and mice, the homologs of *tll*, *l'sc*, and *ems* are expressed in these neuroblasts (Urbach and Technau, 2003), and all three, DLS-2, MASH-1, and EMX-2, are expressed in the subpallial precursors of the mouse basal ganglia (Flames et al., 2007). This degree of correspondence is at least as strong as that seen for the pars intercerebralis/hypothalamus comparison. Thus, as such cases gradually emerge, there may be reason to believe that there is actual correspondence of adult brain regions between flies and mammals. This is not to claim that there will be one-to-one matches; more likely is the possibility that a given region in the far less elaborated fly brain shares common ancestry and functionality with several corresponding vertebrate brain regions. Thus, a comprehensive neural connectivity map in the fly brain could prove to be an invaluable step toward understanding the emergent properties arising from the coordinated activity of large numbers of brain neurons (Alivisatos et al., 2012).

EXPERIMENTAL PROCEDURES

Fly Strains

Flies were maintained under a light:dark 12:12 hr cycle at 25°C. We used Canton-S w^{1118} flies for the generation of the representative CX model. Expression patterns of *Gal4* lines are presented in the Supplemental Information. For visualization of expression, the following transgenic flies were used: (1) *UAS-mCD8::GFP*;*UAS-mCD8::GFP*, (2) *UAS::Dscam[17.1]::GFP*;+;*UAS-Syt::HA*, (3) hs-*FLP*,*FRT*^{19A},*tubP-GAL80*;+; *UAS-Syt::HA*, and (4) *FRT*^{19A},*UAS-mCD8::GFP*;+;+. The *UAS-Syt::HA* (III) line was generated by rejumping the P-element insertion from a starter line (Jefferis et al., 2007). For single-neuron imaging, *GAL4* MARCM transgenic fly lines were heat shocked at 37°C for 10–30 min at the embryonic, larval, or pupal stage.

Sample Preparation

The MARCM technique and whole-mount immunolabeling were carried out as described (Chiang et al., 2011). Brain samples incubated in PBS-T containing one of the following primary antibodies: (1) 1:50 mouse anti-DLG (DSHB), (2) 1:2,000 rabbit anti-HA (Abcam), (3) 1:200 rabbit anti-GABA (Sigma), (4) 1:20 mouse anti-ChAT (DSHB), (5) 1:1,000 rabbit anti-5-HT (Sigma), or (6) 1:100 mouse anti-TH (ImmunoStar) at 4°C for 2 days. After being washed in PBS-T three times, samples were incubated in PBS-T containing one of the following secondary antibodies: (1) 1:200 Alexa-546 anti-mouse (Molecular Probes), (2) 1:250 biotinylated anti-mouse (Molecular Probes), or (3) 1:250 biotinylated anti-rabbit (Molecular Probes) at 4°C for 1 day. Next, brain samples were washed and incubated with 1:500 Alexa Fluor 635 streptavidin (Molecular Probes). Finally, the immunolabeled samples were directly cleared in FocusClear (CelExplorer) for 5 min and then mounted in a drop of MountClear (CelExplorer).

Confocal Imaging

Sample brains were imaged under a Zeiss LSM 510 confocal microscope with 40× or 63× objective lens and following the standard operating procedure as described previously (Chiang et al., 2011). The following settings were used in image the representative CX model acquisition: 633 nm HeNe laser scanning speed 6, frame size 1,024 × 1,024, line average four times, zoom 0.7, optical slice 0.75 μm for 63× lens (N.A. value 1.4). The corrected voxel size of x:y:z is 0.18 × 0.18 × 0.75 μm.

Postrecording Image Processing

We identified all of the CX components in the DLG channel. A component was considered innervated if it contained any signal from the GFP or Syt::HA channel. Innervation patterns were also manually segmented from each individual GFP- or Syt::HA-labeled neuron with Amira 4.1.2 (Visualization Science Group, Merignac Cedex, France) and compile to the common 3D framework of our representative CX model.

Polarity Analysis

By examining 3D images of ~16,000 single neurons collected in the FlyCircuit, we have identified and scored 526 single neurons with a part or all of their innervation in the PB. The polarity (dendrite versus axon) of these PB neurons was assigned based on three steps of analysis. First, we selected eight *Gal4* lines with preferential innervation in the PB. Using Dscam17.1::GFP as a postsynaptic marker and Syt::HA as a presynaptic marker, we found that in the PB, three *Gal4* lines (*VT49130*, *VT38817*, *VT47318*) have only axons, three *Gal4* lines (*E0330*, *VT27015* and *E0837*) have only dendrites, and two *Gal4* lines (*VT34814* and *VT30297*) have both. Second, using MARCM labeling coupled with the Syt::HA marker, we imaged 136 single PB neurons with labeled axonal terminals from the selected *Gal4* lines. We found that *VT34814* and *VT30297* contain exclusively PB LNs. Third, we assigned polarity to neurons collected in the FlyCircuit if their morphology was similar to the neuron in the selected *Gal4* lines. Notably, 26 (12 types) out of 526 neurons collected in the FlyCircuit (Figure S2E9) were not included in the eight selected *Gal4* lines. These neurons with undefined polarity were not included in our wiring principle analysis.

SUPPLEMENTAL INFORMATION

Supplemental Information includes six figures, two tables, and six movies and can be found with this article online at http://dx.doi.org/10.1016/j.celrep.2013.04.022.

LICENSING INFORMATION

This is an open-access article distributed under the terms of the Creative Commons Attribution-NonCommercial-No Derivative Works License, which permits non-commercial use, distribution, and reproduction in any medium, provided the original author and source are credited.

ACKNOWLEDGMENTS

We thank Tzumin Lee, Gregory S.X.E. Jefferis, BDSC, and the DGRC for strains; Jeng-Wen Huang and Chao-yuan Yeh for initial screening on single neurons of FlyCircuit; DSHB for the 4F3 DLG and 4B1 ChAT antibodies. This work was supported by grants from the National Science Council and Ministry of Education in Taiwan (A.-S.C.), and from NIH, ONR, and the Mathers Foundation (R.J.G).

Received: September 28, 2012
Revised: March 12, 2013
Accepted: April 25, 2013
Published: May 23, 2013

REFERENCES

Alivisatos, A.P., Chun, M., Church, G.M., Greenspan, R.J., Roukes, M.L., and Yuste, R. (2012). The brain activity map project and the challenge of functional connectomics. Neuron *74*, 970–974.

Aonuma, H., and Newland, P.L. (2002). Synaptic inputs onto spiking local interneurons in crayfish are depressed by nitric oxide. J. Neurobiol. *52*, 144–155.

Bargmann, C.I. (2006). Comparative chemosensation from receptors to ecology. Nature *444*, 295–301.

Bayraktar, O.A., Boone, J.Q., Drummond, M.L., and Doe, C.Q. (2010). *Drosophila* type II neuroblast lineages keep Prospero levels low to generate large clones that contribute to the adult brain central complex. Neural Dev. *5*, 26.

Briggman, K.L., and Denk, W. (2006). Towards neural circuit reconstruction with volume electron microscopy techniques. Curr. Opin. Neurobiol. *16*, 562–570.

Chen, C.C., Wu, J.K., Lin, H.W., Pai, T.P., Fu, T.F., Wu, C.L., Tully, T., and Chiang, A.S. (2012). Visualizing long-term memory formation in two neurons of the *Drosophila* brain. Science *335*, 678–685.

Chiang, A.S., Lin, C.Y., Chuang, C.C., Chang, H.M., Hsieh, C.H., Yeh, C.W., Shih, C.T., Wu, J.J., Wang, G.T., Chen, Y.C., et al. (2011). Three-dimensional reconstruction of brain-wide wiring networks in *Drosophila* at single-cell resolution. Curr. Biol. *21*, 1–11.

Daniels, R.W., Gelfand, M.V., Collins, C.A., and DiAntonio, A. (2008). Visualizing glutamatergic cell bodies and synapses in *Drosophila* larval and adult CNS. J. Comp. Neurol. *508*, 131–152.

de Velasco, B., Erclik, T., Shy, D., Sclafani, J., Lipshitz, H., McInnes, R., and Hartenstein, V. (2007). Specification and development of the pars intercerebralis and pars lateralis, neuroendocrine command centers in the *Drosophila* brain. Dev. Biol. *302*, 309–323.

Dun, S.L., Brailoiu, E., Wang, Y., Brailoiu, G.C., Liu-Chen, L.Y., Yang, J., Chang, J.K., and Dun, N.J. (2006). Insulin-like peptide 5: expression in the mouse brain and mobilization of calcium. Endocrinology *147*, 3243–3248.

Durstewitz, D., Seamans, J.K., and Sejnowski, T.J. (2000). Dopamine-mediated stabilization of delay-period activity in a network model of prefrontal cortex. J. Neurophysiol. *83*, 1733–1750.

Flames, N., Pla, R., Gelman, D.M., Rubenstein, J.L., Puelles, L., and Marín, O. (2007). Delineation of multiple subpallial progenitor domains by the combinatorial expression of transcriptional codes. J. Neurosci. *27*, 9682–9695.

Foley, N.C., Grossberg, S., and Mingolla, E. (2012). Neural dynamics of object-based multifocal visual spatial attention and priming: object cueing, useful-field-of-view, and crowding. Cognit. Psychol. *65*, 77–117.

Foltenyi, K., Greenspan, R.J., and Newport, J.W. (2007). Activation of EGFR and ERK by rhomboid signaling regulates the consolidation and maintenance of sleep in *Drosophila*. Nat. Neurosci. *10*, 1160–1167.

Hanesch, U., Fischbach, K.-F., and Heisenberg, M. (1989). Neuronal architecture of the central complex in *Drosophila melanogaster*. Cell Tissue Res. *257*, 343–366.

Heinze, S., and Homberg, U. (2007). Maplike representation of celestial E-vector orientations in the brain of an insect. Science *315*, 995–997.

Heinze, S., and Homberg, U. (2008). Neuroarchitecture of the central complex of the desert locust: Intrinsic and columnar neurons. J. Comp. Neurol. *511*, 454–478.

Heinze, S., and Homberg, U. (2009). Linking the input to the output: new sets of neurons complement the polarization vision network in the locust central complex. J. Neurosci. *29*, 4911–4921.

Heinze, S., and Reppert, S.M. (2011). Sun compass integration of skylight cues in migratory monarch butterflies. Neuron *69*, 345–358.

Heinze, S., and Reppert, S.M. (2012). Anatomical basis of sun compass navigation I: the general layout of the monarch butterfly brain. J. Comp. Neurol. *520*, 1599–1628.

Heinze, S., Gotthardt, S., and Homberg, U. (2009). Transformation of polarized light information in the central complex of the locust. J. Neurosci. *29*, 11783–11793.

Herman, J.P., Tasker, J.G., Ziegler, D.R., and Cullinan, W.E. (2002). Local circuit regulation of paraventricular nucleus stress integration: glutamate-GABA connections. Pharmacol. Biochem. Behav. *71*, 457–468.

Homberg, U. (2008). Evolution of the central complex in the arthropod brain with respect to the visual system. Arthropod Struct. Dev. *37*, 347–362.

Homberg, U., Heinze, S., Pfeiffer, K., Kinoshita, M., and el Jundi, B. (2011). Central neural coding of sky polarization in insects. Philos. Trans. R. Soc. Lond. B Biol. Sci. *366*, 680–687.

Izergina, N., Balmer, J., Bello, B., and Reichert, H. (2009). Postembryonic development of transit amplifying neuroblast lineages in the *Drosophila* brain. Neural Dev. *4*, 44.

Jefferis, G.S., Potter, C.J., Chan, A.M., Marin, E.C., Rohlfing, T., Maurer, C.R., Jr., and Luo, L. (2007). Comprehensive maps of *Drosophila* higher olfactory centers: spatially segregated fruit and pheromone representation. Cell *128*, 1187–1203.

Kong, E.C., Woo, K., Li, H.Y., Lebestky, T., Mayer, N., Sniffen, M.R., Heberlein, U., Bainton, R.J., Hirsh, J., and Wolf, F.W. (2010). A pair of dopamine neurons target the D1-like dopamine receptor DopR in the central complex to promote ethanol-stimulated locomotion in *Drosophila*. PLoS ONE *5*, e9954.

Lee, T., and Luo, L. (1999). Mosaic analysis with a repressible cell marker for studies of gene function in neuronal morphogenesis. Neuron *22*, 451–461.

Li, W., Pan, Y., Wang, Z., Gong, H., Gong, Z., and Liu, L. (2009). Morphological characterization of single fan-shaped body neurons in *Drosophila melanogaster*. Cell Tissue Res. *336*, 509–519.

Lin, H.H., Lai, J.S.Y., Chin, A.L., Chen, Y.C., and Chiang, A.S. (2007). A map of olfactory representation in the *Drosophila* mushroom body. Cell *128*, 1205–1217.

Liu, G., Seiler, H., Wen, A., Zars, T., Ito, K., Wolf, R., Heisenberg, M., and Liu, L. (2006). Distinct memory traces for two visual features in the *Drosophila* brain. Nature *439*, 551–556.

Liu, Q.L., Liu, S., Kodama, L., Driscoll, M.R., and Wu, M.N. (2012). Two dopaminergic neurons signal to the dorsal fan-shaped body to promote wakefulness in *Drosophila*. Curr. Biol. *22*, 2114–2123.

Mao, Z.M., and Davis, R.L. (2009). Eight different types of dopaminergic neurons innervate the *Drosophila* mushroom body neuropil: anatomical and physiological heterogeneity. Front Neural Circuits *3*, 5.

Müller, M., Homberg, U., and Kühn, A. (1997). Neuroarchitecture of the lower division of the central body in the brain of the locust (*Schistocerca gregaria*). Cell Tissue Res. *288*, 159–176.

Nicolai, L.J.J., Ramaekers, A., Raemaekers, T., Drozdzecki, A., Mauss, A.S., Yan, J., Landgraf, M., Annaert, W., and Hassan, B.A. (2010). Genetically encoded dendritic marker sheds light on neuronal connectivity in Drosophila. Proc. Natl. Acad. Sci. USA *107*, 20553–20558.

Olsen, S.R., and Wilson, R.I. (2008). Cracking neural circuits in a tiny brain: new approaches for understanding the neural circuitry of *Drosophila*. Trends Neurosci. *31*, 512–520.

Renn, S.C., Armstrong, J.D., Yang, M., Wang, Z., An, X., Kaiser, K., and Taghert, P.H. (1999). Genetic analysis of the *Drosophila* ellipsoid body neuropil: organization and development of the central complex. J. Neurobiol. *41*, 189–207.

Robinson, I.M., Ranjan, R., and Schwarz, T.L. (2002). Synaptotagmins I and IV promote transmitter release independently of Ca(2+) binding in the C(2)A domain. Nature *418*, 336–340.

Sandeman, D. (1999). Homology and convergence in vertebrate and invertebrate nervous systems. Naturwissenschaften *86*, 378–387.

Seung, H.S. (2009). Reading the book of memory: sparse sampling versus dense mapping of connectomes. Neuron *62*, 17–29.

Strausfeld, N.J., and Seyfarth, E.A. (2008). Johann Flögel (1834-1918) and the birth of comparative insect neuroanatomy and brain nomenclature. Arthropod Struct. Dev. *37*, 434–441.

Strauss, R. (2002). The central complex and the genetic dissection of locomotor behaviour. Curr. Opin. Neurobiol. *12*, 633–638.

Tessmar-Raible, K., Raible, F., Christodoulou, F., Guy, K., Rembold, M., Hausen, H., and Arendt, D. (2007). Conserved sensory-neurosecretory cell types in annelid and fish forebrain: insights into hypothalamus evolution. Cell *129*, 1389–1400.

Tomer, R., Denes, A.S., Tessmar-Raible, K., and Arendt, D. (2010). Profiling by image registration reveals common origin of annelid mushroom bodies and vertebrate pallium. Cell *142*, 800–809.

Triphan, T., Poeck, B., Neuser, K., and Strauss, R. (2010). Visual targeting of motor actions in climbing *Drosophila*. Curr. Biol. *20*, 663–668.

Urbach, R., and Technau, G.M. (2003). Molecular markers for identified neuroblasts in the developing brain of *Drosophila*. Development *130*, 3621–3637.

van Swinderen, B., and Greenspan, R.J. (2003). Salience modulates 20-30 Hz brain activity in *Drosophila*. Nat. Neurosci. *6*, 579–586.

Vitzthum, H., Muller, M., and Homberg, U. (2002). Neurons of the central complex of the locust *Schistocerca gregaria* are sensitive to polarized light. J. Neurosci. *22*, 1114–1125.

Wang, J., Ma, X.J., Yang, J.S., Zheng, X.Y., Zugates, C.T., Lee, C.H.J., and Lee, T. (2004). Transmembrane/juxtamembrane domain-dependent Dscam distribution and function during mushroom body neuronal morphogenesis. Neuron *43*, 663–672.

Wang, Z., Pan, Y., Li, W., Jiang, H., Chatzimanolis, L., Chang, J., Gong, Z., and Liu, L. (2008). Visual pattern memory requires foraging function in the central complex of *Drosophila*. Learn. Mem. *15*, 133–142.

Weir, P.T., and Dickinson, M.H. (2012). Flying *Drosophila* orient to sky polarization. Curr. Biol. *22*, 21–27.

Wernet, M.F., Velez, M.M., Clark, D.A., Baumann-Klausener, F., Brown, J.R., Klovstad, M., Labhart, T., and Clandinin, T.R. (2012). Genetic dissection reveals two separate retinal substrates for polarization vision in *Drosophila*. Curr. Biol. *22*, 12–20.

Wessnitzer, J., and Webb, B. (2006). Multimodal sensory integration in insects—towards insect brain control architectures. Bioinspir. Biomim. *1*, 63–75.

Williams, J.L.D., and Boyan, G.S. (2008). Building the central complex of the grasshopper *Schistocerca gregaria*: axons pioneering the w, x, y, z tracts project onto the primary commissural fascicle of the brain. Arthropod Struct. Dev. *37*, 129–140.

Wilson, R.I. (2011). Understanding the functional consequences of synaptic specialization: insight from the *Drosophila* antennal lobe. Curr. Opin. Neurobiol. *21*, 254–260.

Woods, D.F., and Bryant, P.J. (1991). The discs-large tumor suppressor gene of Drosophila encodes a guanylate kinase homolog localized at septate junctions. Cell *66*, 451–464.

Young, J.M., and Armstrong, J.D. (2010a). Building the central complex in *Drosophila*: the generation and development of distinct neural subsets. J. Comp. Neurol. *518*, 1525–1541.

Young, J.M., and Armstrong, J.D. (2010b). Structure of the adult central complex in *Drosophila*: organization of distinct neuronal subsets. J. Comp. Neurol. *518*, 1500–1524.

Yu, H.H., Chen, C.H., Shi, L., Huang, Y.L., and Lee, T.M. (2009). Twin-spot MARCM to reveal the developmental origin and identity of neurons. Nat. Neurosci. *12*, 947–953.